CO_2 Laser Welding of Low-Density Polyethylene for Soft Linear Eversion Robot Fabrication

Brandon Saldarriaga, Carlo A. Seneci, S.M.Hadi Sadati, Zicong Wu, Kawal Rhode, and Christos Bergeles

***Abstract*— Vine soft robots navigate through apical extension by everting material stored at their base. They are demonstrating promise in an increasing number of surgical applications, thanks to their intrinsic softness and reduced friction while navigating through the surrounding anatomical structures. State-of-the-art fabrication of linear eversion elements uses modified heat sealers to approximate Low-Density Polyethylene (LDPE) layers and form the everting tubes. However, the weld tracks are wide, and only straight elements have been produced. Our paper proposes and evaluates the fabrication of the everting elements of soft linear vine robots by employing CO2 laser welding of double-layer Low-Density Polyethylene (LDPE) films. Our approach can manufacture everting elements with reduced weld track and, ultimately, of complex patient-specific shapes. Specifically, our paper enhances the weld quality by studying and optimising the welding variables and introducing a Zinc Selenide (ZnSe) window to obtain uniform and robust welds. A comparison between the weld strength of state of the art heat sealers and the proposed approach was performed, proving that is possible to retain comparable weld strength whilst reducing the weld size, thereby enabling the manufacture of smaller vine everting robots. The paper concludes by showcasing the eversion of a 7cm-long growing element manufactured using the proposed method as a proof of concept.**

I. Introduction

Vine soft-robots [1] emulate plant growth by elongating from their tip through pressure-based eversion of a sleeve-like tubular structure [2]. Vine robots' softness enables them to navigate cluttered and fragile environments, e.g. for search and rescue [3], intraluminal interventions [4], endovascular surgery [5], archaeology [6] and coral reef exploration [7].

Key requirements for everting element materials include biocompatibility, disposability, lightweightness and burst resistance. For system miniaturisation, material thickness must be minimal to provide the largest possible lumen for a given diameter. Consequently, thin polymer sheets emerge as a viable option for the construction of everting robots.

Elastane, a stretchable fabric, and Thermoplastic Polyurethane (TPU), have been explored in growing robots [8]. An alternative, Low-Density Polyethylene (LDPE), a thermoplastic polymer belonging to the polyethylene family, used in [9], [10], [11], [12], [4], [13], exhibits low density, high flexibility, and excellent chemical resistance. With a temperature resistance up to 65 °C and capacity to withstand pressures up to 14 kPa [14], LDPE is gaining attention as the material of choice for linear eversion sheaths.

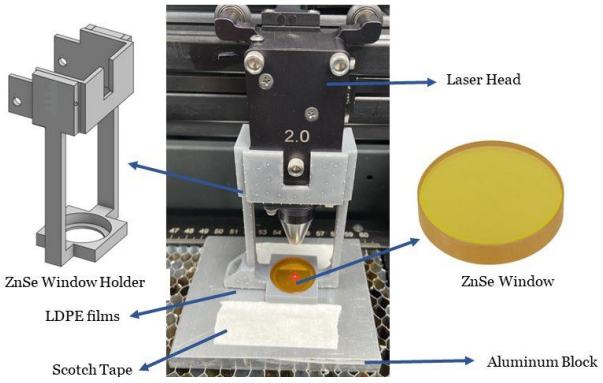

Fig. 1: Our setup embedded within an off-the-shelf CO_2 laser cutter (Universal Laser Systems, 10.6 μm, 60W, VLS4.60 series) including a Zinc Selenide (ZnSe) circular broadband precision window (WG70530-D, Thorlabs). 3D CAD model for the laser head mount with a circular slot for theZnSe window.

While LDPE tubes of various diameters can be procured, there is merit in developing in-house LDPE sheet approximation techniques to support patient-specific eversion elements [5], experimentation with new materials, self-sensing etc. [9]. In our prior work [4], [13], we used a modified plastic heat sealer to approximate and seal two pieces of LDPE. This method led to the creation of everting elements of 2.9 mm diameter, among the smallest published, but with everting length of 8 cm due to workspace limitations. Furthermore, the approach could only produce straight tubes, had a large weld seam of 1.45 mm per seam, and was limited in the length of the welded elements. Other fabrication methods use a flexible urethane-coated ripstop nylon. The nylon fabric is cut into a tapered shape, sealed and cured into a narrow tube with polyurethane glue, then shaped using a U-shaped mould [5]. However, this method would lead to tearing and stretching of the LDPE due to its material properties. Ultrasonic welding, a form of friction welding, employs pressure and high-frequency, low-amplitude vibrations to bond materials together. It is well-suited for vine robots made of TPU-coated ripstop nylon but led to a high material fail-rate when applied to LDPE at the thickness used [15].

Conversely, CO_2 laser welding offers high precision

This work was supported by the Wellcome/EPSRC Centre for Medical Engineering [WT203148/Z/16/Z] and by Innovate UK under the Horizon Europe Guarantee Extension [10062486]. B. Saldarriaga was supported by King's Centre for Doctoral Training on Surgical and Interventional Engineering. Z. Wu received support from China Scholarship Council (CSC No.:202008060101). For the purpose of open access, the author has applied for a CCBY licence to any Author Accepted Manuscript version arising from this submission.

All authors are with the School of Biomedical Engineering & Imaging Sciences, King's College London, UK. Correspondence: brandon.saldarriaga@kcl.ac.uk

and accuracy for rapid prototyping or intricate shapes and downtime reduction, essential for quicker system integration. Building on preliminary evidence in [16], [17], and numerical analysis in [18], we propose addressing these challenges using CO_2 laser-based welding of LDPE films, but without requiring additives or lower wavelengths and with high weld strength and reduced weld seam dimensions for repeatable everting element fabrication.

The paper presents our setup alongside meticulous experimentation with various laser parameters, the regulation of which is crucial to achieve successful welds of $30\,\mu$m thick LDPE sheets.

II. Materials and Experimental Setup

Laser Transmission Welding (LTW) of polymers has been used since the 1970s [19]. In LTW, a laser beam is irradiated onto overlapping polymer parts. The upper part is commonly laser-transparent, and the lower part is laser-absorbent. The laser beam irradiates and welds the materials together. When welding two transparent materials, it is common to use IR-absorbing intermediate layers, or additives, for improved laser absorbance and inherently laser welding [20]. However, through the use of ZnSe heatsinks and a defocused Gaussian beam profile (also known as a "top hat"), the necessity of IR-absorbing pigments or dyes is removed [17].

The choice of laser is crucial for effective welding, especially considering that most polymers absorb CO2 laser radiation [21], which operates at a wavelength of $10.6\,\mu$m, penetrating to a small depth within the substrate. CO_2 laser welding involves controlling several parameters to achieve optimal weld quality between two materials, including laser power, Pulses Per Inch (PPI), welding speed, beam diameter, clamping force, standoff distance[1], and the number of scans [21]. These parameters must be adjusted based on the material type, thickness, and desired weld characteristics. Even the laser's in-built ventilation can have a detrimental effect on the weld. Therefore, parameter optimization is crucial to ensure proper heat input and to avoid material perforation, irregular welds, bubble formation, and weld-seam break. These challenges are exacerbated when the thin $30\,\mu$m LDPE films comprising the everting element of intraluminal vine robots are considered.

Our work focuses on creating thin, airtight, and effective weld seams that enable linear everting elements of the reduced seam width without compromising integrity. Our comparator will be the performance of linear everting elements created with the method of [4], i.e., heat sealing.

A. Material Choice

LDPE exhibits an absorbance of only 10% [16]; only a small percentage of the delivered energy contributes to welding. With a degree of crystallinity of 60%, LDPE indicates promising weld strength, as higher degrees of crystallinity correlate with a higher melt flow index, enabling high weld strength [16] despite low absorption.

We utilize LDPE polymer films supplied by Polybags Ltd, UK, with a thickness of $30\mu m$ (120 gauge), meeting the minimum thickness requirement for welding determined by numerical analysis ($20\mu m$) in [18].

B. CO_2 Laser Welding Setup

The LDPE film rolls are cut into $5\,\text{cm}\times3\,\text{cm}$ segments, an area that facilitates multiple consecutive tests and rapid detection of defective welding while minimizing experimentation time and maximizing material utilization. Successful welds of this length can validate the proposed manufacturing method before embarking on full-length growing sheath creation. As irregularities can adversely impact the bonding process, preparation of the LDPE material is conducted to eliminate dust residue by blowing medical compressed air for $1-2\,\text{s}$ on the polymer segments. A visibly clean and smooth film section is selected for experimentation.

A $100\,\text{mm}\times80\,\text{mm}$ aluminium block of $10.65\,\text{mm}$ thickness is positioned on the cutting bed to act as a final homogeneous absorption surface of the laser beam, i.e. the substrate (see Fig. 1). The block also dissipates heat away from the bottom of the polymer, offering bottom-heavy support, thereby ensuring uniform proximity of the LDPE to the laser beam without causing pits or curved regions on the material.

To facilitate welding, the two LDPE films are horizontally stacked and tensioned using tape along their perimeters against the aluminium block. The sample is positioned on the block to permit plastic shrinkage perpendicular to the welding direction, enhancing contact between the films and increasing bonding surface area as seen in Fig. 1.

The 2D shape design for the CNC laser cutter is prepared using AUTOCAD (2023)[2]. In the first instance, a $4\,\text{cm}$ line represents the intended weld. Subsequently, sheaths of $7\,\text{cm}$ eversion length and $5\,\text{mm}$ in diameter were designed. The flexibility of everting robot shapes that can be achieved with laser-based welding is our primary motivation.

III. Experiment Design

The experimental protocol involves a coarse laser-parameters sweep, finer parameter assessment, laser beam profile shaping, evaluation of tensile strength, and final pressure-based eversion evaluation of a manufactured sheath. Our approach is presented in what follows, with results presented in Sec. IV.

A. Coarse Parameter Sweep

A coarse laser parameter sweep was carried out with visual observation of acceptable welds. We evaluated CO_2 welding parameters in order of importance [22], namely power, standoff distance, and speed. We also considered PPI, i.e., energy deposition per inch, which, even though not emphasized in the literature for welding LDPE films, influences the temperature profile and, ultimately, weld strength. The results were used to find the working narrow range of each parameter.

[1]The standoff distance will also be referred to as Z-displacement.

[2]https://web.autocad.com

Laser power: Starting from the manufacturer recommended values for 1 mm thick Polypropylene (PP) experiments were conducted by varying the power level in steps of 10%, ranging from 10% to 100% (60W), followed by the narrow range exploration at steps of 1%.

Standoff distance: Experiments involved incrementally increasing the distance between the laser head and sample by 1 mm, until imperfect welding was observed, for the best power value identified above. The narrow range experiments were carried out with steps of 0.1 mm increments.

Weld speed: Experiments kept the power and stand-off distance pair-wise constant. Speed was adjusted in 10% intervals, ranging from 10% to 100%, until either melting or incomplete welding was observed. Once the smaller range was identified we used 1% increments.

PPI: With low PPI, weld spots are not overlapping, permitting thermal conduction to join areas between them. By measuring spot size under the microscope, the possible number of weld spots within a given weld line could be calculated. The high PPI approach commenced from the PP parameters established earlier, along with the determined power and weld speed values. The PPI settings tested ranged from 10 to 1000 pulses per inch, increasing initially in increments of 100 and subsequently in increments of 10.

B. Weld Seam Optimization

The identified narrow range of laser parameters was assessed to optimize the weld based on optical microscopy characterization (Olympus, BX53M) and ensure the absence of large holes, excessive thermal damage, air bubbles, and any weld inhomogeneity. A total of 10 welds were manufactured at each iteration within the narrow range of each welding parameter: 5 welds at 3 cm, and 5 welds at 6 cm from the extractor, enabling to also understand the effect that the distance to extractor has on track width.

Each weld was visually assigned a quality number: **(1)** No weld; **(2)** Weld follows an unwelding pattern or exhibits thermal damage; **(3)** Weld is weak or exhibits large unwelded areas; **(4)** Welds with few unwelded regions and resistant to hand-pulling forces; **(5)** Weld with no unwelded regions and resistant to hand-pulling forces.

C. Beam Profile Shaping

Heat distribution at the polymers' interface is an additional design parameter. Top hat beams offer uniform irradiance across the laser beam cross-section. Due to their steeper transition, they enable more effective energy distribution and smaller Heat Affected Zone (HAZ) than Gaussian beams, which exponentially decay from the axis to zero intensity [23], thereby potentially causing overheating and degradation in the weld centre.

As thin polymers absorb CO_2 laser radiation (at $10.6\,\mu$m wavelength) in a shallow depth within the substrate [21], it is critical to improve the irradiance across their surface by transforming Gaussian beam profiles into top-hat ones.

D. ZnSe Window Implementation

To further enhance energy distribution and prevent thermal damage a one-inch diameter ZnSe circular broadband precision window (Thorlabs, UK) was used to promote bonding within the inter-layer of the LDPE films.

The circular window was placed in the slot of a 3D printed mount (see Fig. 1), which securely held onto the laser head, fastened in place by an m4 screw and two nuts on either side at the posterior part of the design. Its design ensured straightforward alignment, stability of the window throughout the welding process, and its proximity almost in contact with the surface of the LDPE films.

E. Tensile Strength Evaluation and Deployment

For each of the high-quality welds created, a second pass is carried out to increase weld strength and ensure all areas of the joint have been successfully fused together. The last step entailed quantitative evaluation of weld strength by performing tensile strength tests (Instron, 5969 dual column with a 500N load cell) perpendicular to the direction of the weld. A comparative analysis was undertaken between 10 samples of the optimal weld generated from the CO_2 laser welding technique, and a set of 10 control welds fabricated using the modified plastic heat sealer method established in [4], FS-300 heat sealer (Yontree, China); where the stop criteria was a 40% reduction from the maximum force.

Finally, the developed sheath was deployed within the setup of [13] and eversion was evaluated.

IV. Experimental Results

Here, we present and analyse the results from the experiments with the CO_2 laser welding of a double LDPE layer.

A. Coarse Parameter Sweep

Laser power: Thermal damage was observed at higher power levels, above 70%. This was attributed to increased energy deposition from the laser beam, leading to excessive heat generation. At lower levels, below 20%, insufficient energy was deposited; hence, there is no bonding between both LDPE layers. The power range 35% to 40% produced a visually identified weld, even with some imperfections, and was identified as relevant for finer investigation.

Standoff distance: Increased Z-displacement defocused the laser beam, forming a larger and wider elliptical beam spot [24]. This requires less power to achieve the critical energy density for effective welding, resulting in a more uniform energy distribution and enhancing weld strength. The acceptable range was identified to be: 26.8 mm to 27.8 mm.

Weld speed: Low welding speeds have the disadvantage that, for this LDPE film thickness, the risk of thermal damage (see Fig. 2b) as both weld depth and width increase. Lower speed allows for increased interaction time but risks overheating and degradation. Therefore, faster welding speeds are preferable for these LDPE films. Too high welding speeds decreased interaction time with the material and minimized heat input, resulting in weak or non-welds (See Fig. 2a).

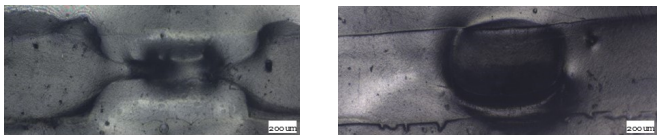

(a) (b)

Fig. 2: Weld morphology showing (a) areas of non-welded regions, and (b) areas with damaged weld sections.

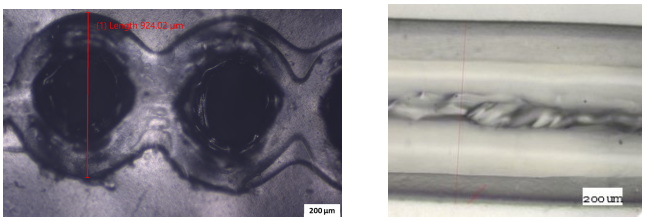

(a) (b)

Fig. 3: Weld morphology through exploring both PPI approaches. a) Depicts the results from the low PPI approach. b) Depicts the results from the high PPI approach.

The results indicate that the narrow range experiments are in between 65% to 75%.

PPI: Two different approaches, low PPI and high PPI, were trialed as described in Section III-A. Fig. 3a shows CO_2 laser welding of two LDPE films using the low PPI method, with the largest track width measuring $841\,\mu$m.

Conversely, Fig. 3b illustrates the high PPI approach, with a mean track width of $900\,\mu$m.

Complete line welding using the low PPI method relies on efficient heat conduction between points. Hence, inadequate heat deposition results in insufficient residual heat for thermal conduction between adjacent points, leading to non-uniformities in the weld. Thermal adhesion areas are visible, and closely spaced weld points connect due to material expansion (see Fig. 3a). This halves the weld's resisting cross-section, raising concerns for applications needing hydraulic/pneumatic encapsulation. The highest points of low PPI welds have a thickness of $841\,\mu$m, smaller than those made with a modified heat sealer (Fig. 6b).

In contrast, the high PPI experiments demonstrate a more uniform weld, with no deformities along the edge of the welded region (Fig. 3b). The central longitudinal section exhibits a strongly bonded area, suggesting a robust bond between the material layers. However, moving away from the middle line in the longitudinal plane, varying grey areas between the weld edges and the central welded section indicate non-uniform weld morphology, likely due to the elongated wings of the Gaussian beam resulting in an extended HAZ and darker regions on the sides of the weld. Overall, this suggests non-homogeneous weld morphology in the radial direction, leading to irregularities in regions where the minimum energy threshold for effective welding has not been met. As the high PPI was shown to deliver a more uniform result, this method was explored further in the narrow range; which was found to be from 500 to 600 PPI.

B. Weld Seam Optimization

Fig. 4 displays the results of LDPE film welding within a narrow parameter range, illustrating the independent impact of parameter alteration on weld quality based on the visual quantification system outlined in Section III-B. Additionally, the influence of small-range parameter fluctuations on track width is depicted in Fig. 5, with red and blue data points representing distances of $3\,$cm and $6\,$cm from the laser extractor, respectively.

Higher power density increases weld penetration depth, enlarging the weld pool and ultimately the weld width [25]. Optimal power values fall within the range of 35% to 40%. Results in Fig. 4a show better weld quality at 39% power, exhibiting high frequency and low variance. The range between 37% and 39% power exhibits higher track width, consistent with the weld quality in the contour plot (Fig. 4a), indicating a better weld profile and improved weld seam, however, larger track widths. At 39% power, the track width ranges between $580\,\mu m$ and $760\,\mu m$ (see Fig. 5a).

Speed range between 65% and 75% shows promising results in weld quality. Conversely, as welding speed increases, track width decreases, with the lowest track width observed at 73% speed. Lower speeds result in longer laser irradiation time, increasing weld pool and depth within the material [26]. Fig. 4b highlights the optimal welding speed at 70%, displaying low variance and high weld quality, corresponding to a track width range of 580-760 μm as seen in Fig. 5b.

Fig. 4c illustrates that the optimal range for the PPI parameter is between 500 and 600. Higher PPI values lead to a higher thermal load during welding, resulting in more energy being delivered within the same line energy. This can cause the melting and rupture of the polymer films. Conversely, lower values do not deliver the necessary line energy to successfully weld both layers without creating multiple gaps. Notably, at 540 PPI indicates high-frequency values of good weld rating and low variance while exhibiting the lowest track width range at 600-720 μm.

The value with the smallest variance and high weld rating for Z-displacement is found at 27.8 mm (Fig. 4d), where the true displacement is 17.13 mm (accounting for the aluminium support plate). This finding suggests that the laser beam is sufficiently defocused, resulting in a more uniform energy distribution within the laser spot and reducing the energy gradient. Fig. 5d, Z-displacement demonstrates little effect between the range of 26.8 mm-27.8 mm. However, comparing the better weld quality results from Fig. 4d, where the best result is at 27.8 mm, shows a narrower track width range of 580-740 μm.

Fig. 5 suggests that samples welded 6 cm away from the extractor generally have smaller track widths compared to those at 3 cm, possibly due to stronger airflow near the extractor affecting heat distribution during welding. However, within the narrow parameter range, changes do not significantly impact track width, likely because the range is

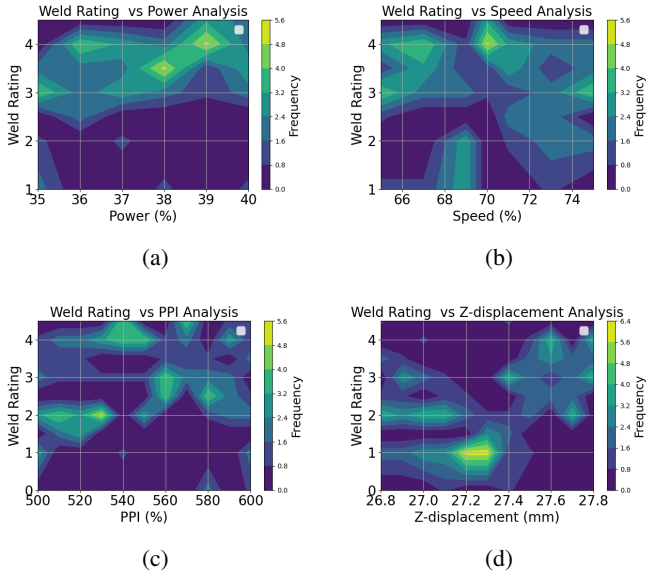

Fig. 4: The effect of each of the welding parameters on Weld Quality over a large range of values. (a) Power (b) Speed (c) PPI (d) Z-displacement.

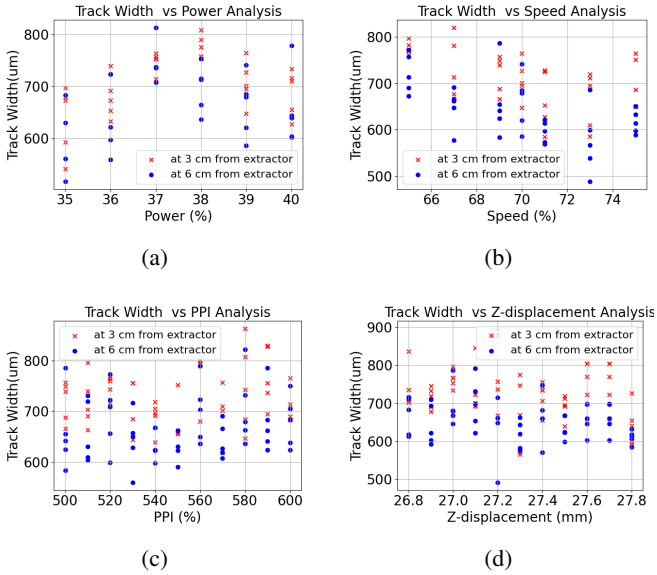

Fig. 5: The effect of small changes of the welding parameters on the weld track width. (a) Power (b) Speed (c) PPI (d) Z-displacement.

too narrow for major differences. The parameters yielding the best weld quality are retained as follows: Power: 39%, Speed: 70%, PPI: 540, Z-displacement: 27.8 mm. These values are selected for manufacturing a complete everting element.

C. ZnSe Window Implementation

Irregular welding poses risks such as trapping bubbles, which can harm hermetic properties and joint fatigue strength [25]. Medical devices strictly prohibit fume bubbles due to air embolism risks. Even with defocused Gaussian beams (i.e. "Top-hat beam"), high energy peaks persist at the centre necessitating ZnSe window implementation post weld seam optimization.

Despite optimizing parameters and achieving improved welding, small unwelded gaps persist. The absence of film contact before welding leads to non-homogeneity along the weld, making effective welding challenging across repeated experiments. Further parameter adjustments are unlikely to enhance results. Introducing clamping pressure as another parameter ensures continuous material contact.

To address this, the ZnSe window is placed in close proximity to the film surface, at a distance of 0.2 mm. This setup allows the window to hover above the films, reducing thermal damage and enabling the weld pool to develop within the interlayer of the polymer films. Expanding the melting pool size enhances gap-bridging capability and creates a more uniform temperature distribution in the weld zone, resulting in an improved final weld seam that bridges the gaps between the layers. Fig. 6a shows the microstructural differences in the weld morphology with the ZnSe window implementation compared to without (see Fig 3b). The ZnSe window implementation leads to nearly optimal weld characterization. Strong welds and consistent results were

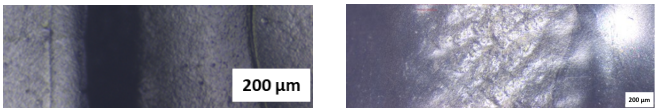

Fig. 6: Resulting weld morphology through exploring the implementation of (a) the ZnSe window and (b) the modified heat sealer from [4].

indicated by the absence of trapped air bubbles and minimal deformities along the edge of the welded region.

D. Tensile Strength Evaluation and Deployment

The graph in Fig. 7 illustrates the applied force (N) and displacement (mm) relationship for the weld seam of the laser welded samples (See Fig. 7b) and the control weld samples (See Fig. 7a). Table I presents the average results of the tensile strength test. Lap joint strength is commonly measured as maximum force [N], representing the maximum force the material withstands at the point of failure. The laser welding average is found to be 12.55 $\pm$ 1.15 N, compared to the control average at 13.92 $\pm$ 1.64 N, indicating an 11% decrease in joint strength. The stress level at which plastic deformation begins, tensile stress at yield [MPa], was 4.18 $\pm$ 0.38 MPa, whereas the control sample measured at 4.62 $\pm$ 0.62 MPa. These results indicate comparable stress endurance between both sample sets, suggesting repeatability in laser-welded sample production for soft-growing robot manufacture. It is worth noting the weld seam reduction from the control's average of 1479 μm to 857 μm in the laser welded samples, which allows us to fabricate smaller everting elements and target smaller anatomical lumen.

For growing robot applications where the material may deform under pressure changes, the tensile displacement at

TABLE I: Averaged tensile strength tests.

Sample	Max. Force [N]	Tensile Displacement at Max. Force [MPa]	Tensile Stress at Yield (Zero Slope)[MPa]
Control	13.92 ± 1.64	10.19 ± 6.16	4.62 ± 0.62
CO_2 Laser Welding	12.55 ± 1.15	3.41 ± 0.74	4.18 ± 0.38

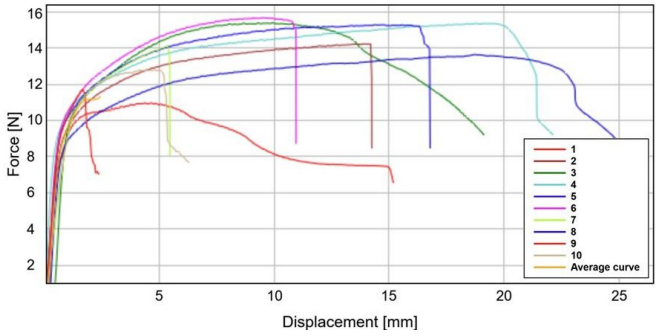

(a)

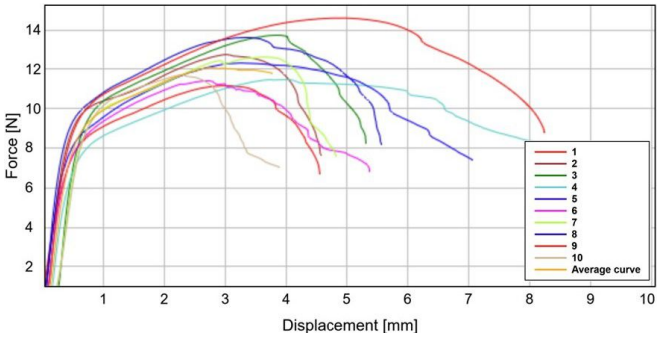

(b)

Fig. 7: Force applied (N) vs displacement (mm) of: (a) control sample manufactured using the heat sealer of [4] 10 samples, and (b) the CO_2 laser welding method over 10 samples.

maximum force [MPa] is analyzed, indicating the maximum deformation the specimen undergoes. This parameter averaged at 3.41 ± 0.74 MPa for the laser-welded samples, compared to 10.19 ± 6.16 MPa for the control samples. The substantial difference is likely due to bulk substrate failure observed in all control samples, resulting in tensile yield and break, evident by the sudden drop before breaking in Fig. 7a. In contrast, only 60% of the laser-welded samples demonstrated substrate failure, albeit with more plastic deformation post-failure, indicating a less brittle outcome. This implies that the laser-welded everting elements would not burst during their deployment, but rather gradually leak, resulting in a drop of pressure that can be recorded by the actuation system.

E. Soft Growing Robot Fabrication

The method outlined in this paper was used to create a 20 cm length sheath for a 5 mm diameter, soft everting element, allowing up to 7 cm eversion factoring in length "sacrificed" to attach the eversion element to a pressurization chamber. Fig. 8 demonstrates the resulting everted sheath, showcasing effective and airtight welding. All five manufactured everting sheaths demonstrated successful eversion. Two out of five everting sheaths fully everted without any leaks, while three prototypes leaked and eversion halted. This number is comparable with the performance of everting sheaths manufactured with the control (heat sealer) approach, wherein three out five sheaths fully everted, while two leaked. This comparison highlights the practical trade-off of the reduced track width and tensile strength differences on the eversion process, and guides our future investigations.

Fig. 8: Eversion of an 7 cm growing robot manufactured using the CO_2 laser welding method, everting with the actuation system of [13].

V. Conclusion

This paper proposed laser-based fabrication of the everting elements of soft-growing robots from LDPE. Weld heat distribution was improved by employing CO_2 laser welding and optimizing laser parameters, along with implementing a ZnSe heatsink window, resulting in optimal weld quality with minimal defects and no trapped air bubbles. Small differences in joint strength between the in-lab heat sealer and the CO_2 laser welding method alongside a 42% track width reduction lead to a lower eversion success rate at only 40% compared to the control at 60%. The resulting everting elements were deployed within an actuation system, showcasing the way forward to creating patient-specific everting elements with varying diameters and properties.

The proposed manufacturing approach opens the way to investigate new profiles for everting elements, including patient-specific designs, while pushing the size of the everting elements towards the millimetre diameter domain.

VI. Acknowledgments

We would like to thank Helge A. Wurdemann, Dipl.-Ing., PhD Professor, UCL Mechanical Engineering University College London (UCL) and Ray Hoang, Laboratories Technician, Materials and Structures, University College London (UCL), for their help with tensile strength testing.

Acronyms

HAZ Heat Affected Zone. 3, 4

LDPE Low-Density Polyethylene. 1–4, 6

LTW Laser Transmission Welding. 2

PP Polypropylene. 3

PPI Pulses Per Inch. 2–5

TPU Thermoplastic Polyurethane. 1

ZnSe Zinc Selenide. 1–3, 5, 6

REFERENCES

[1] E. W. Hawkes, L. H. Blumenschein, J. D. Greer, and A. M. Okamura, "A soft robot that navigates its environment through growth," *Science Robotics*, vol. 2, no. 8, 7 2017. [Online]. Available: https://www.science.org/doi/10.1126/scirobotics.aan3028

[2] L. H. Blumenschein, M. M. Coad, D. A. Haggerty, A. M. Okamura, and E. W. Hawkes, "Design, Modeling, Control, and Application of Everting Vine Robots," *Frontiers in Robotics and AI*, vol. 7, p. 153, 11 2020.

[3] H. Tsukagoshi, N. Arai, I. Kiryu, and A. Kitagawa, "Smooth creeping actuator by tip growth movement aiming for search and rescue operation," pp. 1720–1725, 2011.

[4] P. Berthet-Rayne, S. M. Sadati, G. Petrou, N. Patel, S. Giannarou, D. R. Leff, and C. Bergeles, "Mammobot: A miniature steerable soft growing robot for early breast cancer detection," *IEEE Robotics and Automation Letters*, vol. 6, no. 3, pp. 5056–5063, 7 2021.

[5] M. Li, R. Obregon, J. J. Heit, A. Norbash, E. W. Hawkes, and T. K. Morimoto, "Vine catheter for endovascular surgery," *IEEE Transactions on Medical Robotics and Bionics*, vol. 3, no. 2, pp. 384–391, 2021.

[6] M. M. Coad, L. Blumenschein, S. Cutler, J. Zepeda, N. Naclerio, H. El-Hussieny, U. Mehmood, J. Ryu, E. Hawkes, and A. Okamura, "Vine robots: Design, teleoperation, and deployment for navigation and exploration," *IEEE Robotics Automation Magazine*, 2020.

[7] J. Luong, P. Glick, A. Ong, M. S. deVries, S. Sandin, E. W. Hawkes, and M. T. Tolley, "Eversion and retraction of a soft robot towards the exploration of coral reefs," in *2019 2nd IEEE International Conference on Soft Robotics (RoboSoft)*, 2019, pp. 801–807.

[8] C. Suulker, S. Skach, and K. Althoefer, "Integrating elastic bands to enhance performance for textile robotics," 2023.

[9] J. D. Greer, T. K. Morimoto, A. M. Okamura, and E. W. Hawkes, "A Soft, Steerable Continuum Robot that Grows via Tip Extension," *Soft Robot*, vol. 6, no. 1, pp. 95–108, 2019.

[10] I. Exarchos, K. Wang, B. H. Do, F. Stroppa, M. M. Coad, A. M. Okamura, and C. K. Liu, "Task-Specific Design Optimization and Fabrication for Inflated-Beam Soft Robots with Growable Discrete Joints," *Proceedings - IEEE International Conference on Robotics and Automation*, pp. 7145–7151, 2022.

[11] H. El-Hussieny, U. Mehmood, Z. Mehdi, S. G. Jeong, M. Usman, E. W. Hawkes, A. M. Okarnura, and J. H. Ryu, "Development and Evaluation of an Intuitive Flexible Interface for Teleoperating Soft Growing Robots," *IEEE International Conference on Intelligent Robots and Systems*, pp. 4995–5002, 12 2018.

[12] L. H. Blumenschein, L. T. Gan, J. A. Fan, A. M. Okamura, and E. W. Hawkes, "A Tip-Extending Soft Robot Enables Reconfigurable and Deployable Antennas," *IEEE Robotics and Automation Letters*, vol. 3, no. 2, pp. 949–956, 4 2018.

[13] Z. Wu, M. D. I. Reyzabal, S. Sadati, H. Liu, S. Ourselin, D. Leff, R. K. Katzschmann, K. Rhode, and C. Bergeles, "Towards a physics-based model for steerable eversion growing robots," *IEEE Robotics and Automation Letters*, vol. 8, no. 2, pp. 1005–1012, 2023.

[14] M. M. Coad, L. H. Blumenschein, S. Cutler, J. A. R. Zepeda, N. D. Naclerio, H. El-Hussieny, U. Mehmood, J.-H. Ryu, E. W. Hawkes, and A. M. Okamura, "Vine Robots," *IEEE Robotics & Automation Magazine*, vol. 27, no. 3, pp. 120–132, 2020.

[15] N. Agharese and A. M. Okamura, "Configuration and fabrication of preformed vine robots," Submitted. [Online]. Available: https://arxiv.org/abs/2306.01166

[16] J. P. Coelho, M. A. Abreu, and M. C. Pires, "High-speed laser welding of plastic films," *Optics and Lasers in Engineering*, vol. 34, no. 4-6, pp. 385–395, 10 2000.

[17] S. K. Kurosaki Yasuo, Matayoshi Tomoya, "A novel CO2 laser welding of plastics using a transparent solid heat sink without causing thermal damage," 3 2006.

[18] G. Casalino and E. Ghorbel, "Numerical model of CO2 laser welding of thermoplastic polymers," *Journal of Materials Processing Technology*, vol. 207, no. 1-3, pp. 63–71, 10 2008.

[19] H. Silvus Jr and S. Wachtell, *Perforating, welding, and cutting plastic films with a continuous CO2 laser*, 1970.

[20] B. Acherjee, A. S. Kuar, D. Misra, and S. Mitra, "Laser transmission welding of thermoplastics: An overview of experimental findings–process, development and applications," *Journal of Manufacturing Technology Research*, vol. 3, no. 3/4, p. 211, 2011.

[21] B. Acherjee, "Laser transmission welding of polymers – a review on process fundamentals, material attributes, weldability, and welding techniques," *Journal of Manufacturing Processes*, vol. 60, pp. 227–246, 2020. [Online]. Available: https://www.sciencedirect.com/science/article/pii/S152661252030685X

[22] B. Acherjee, A. S. Kuar, S. Mitra, and D. Misra, "Empirical Modeling and Multi-Response Optimization of Laser Transmission Welding of Polycarbonate to ABS," *Lasers in Manufacturing and Materials Processing*, vol. 2, no. 3, pp. 103–123, 9 2015. [Online]. Available: https://link.springer.com/article/10.1007/s40516-015-0009-0

[23] L. F. Gonçalves, F. M. Duarte, C. I. Martins, and M. C. Paiva, "Laser welding of thermoplastics: An overview on lasers, materials, processes and quality," *Infrared Physics & Technology*, vol. 119, p. 103931, 12 2021.

[24] J. M. Coelho, M. A. Abreu, and F. Carvalho Rodrigues, "Modelling the spot shape influence on high-speed transmission lap welding of thermoplastics films," *Optics and Lasers in Engineering*, vol. 46, no. 1, pp. 55–61, 2008. [Online]. Available: https://www.sciencedirect.com/science/article/pii/S0143816607001236

[25] B. Acherjee, "Laser transmission welding of polymers – a review on welding parameters, quality attributes, process monitoring, and applications," *Journal of Manufacturing Processes*, vol. 64, pp. 421–443, 2021. [Online]. Available: https://www.sciencedirect.com/science/article/pii/S1526612521000414

[26] D. M. Douglass and C.-Y. Wu, "Laser welding of polyolefin elastomers to thermoplastic polyolefin," in *International Congress on Applications of Lasers & Electro-Optics*. AIP Publishing, 2003.